Advanced Journal of Chemistry-Section A, 2020, 3(4), 408–421
Available online at : www.ajchem-a.com
ISSN Online: 2645-5676
DOI: 10.33945/SAMI/AJCA.2020.4.3

Original Research Article

Adsorption and Photocatalytic Removal of Arsenic from Water by a Porous and Magnetic Nanocomposite: $Ag/TiO_2/Fe_3O_4$@GO

Marzieh Miranzadeh[a], Fahime Afshari[b], Behnoosh Khataei[c], Mohammad Zaman Kassaee[a,*]

[a] *Department of Chemistry, Tarbiat Modares University, P.O. Box 14155-4838, Tehran, Iran*
[b] *Industrial paints of Iran Co., Isfahan, Iran*
[c] *Department of Civil and Environmental Engineering, Tarbiat Modares University, Tehran, Iran*

ARTICLE INFO

Received: 30 September 2019
Revised: 13 November 2019
Accepted: 04 December 2019
Available online: 08 December 2019

KEYWORDS

Arsenic
Adsorption
Photocatalyst
Magnetic nanocomposite
Ag nanoparticles

ABSTRACT

As (III) regularly requires oxidation to As (V), before it can be removed from water. Here, we reported photocatalytic removal of As (III) as well as adsorption of As (III) and As (V) using a novel, porous magnetic $Ag/TiO_2/Fe_3O_4$@GO nanocomposite which was characterized *via* FT-IR, XRD, SEM, and TEM. A mathematical model (the central composite design) was used to estimate the relationship between the observed adsorption and our set of variables including initial concentration of arsenic ions, adsorbent dosage, pH, and the contact time. An optimum adsorption capacity of about 91% was observed for As (III) using 20 mg adsorbent with 24 ppm initial concentration of As (III), at pH = 5, within 90 min, and room temperature. Likewise, an optimum adsorption capacity of about 87% was observed for As (V) using 11 mg adsorbent with 17 ppm initial concentration of As (V), at pH = 3, within 30 min, and room temperature. The electrostatic factors between surface charge of nanocomposite and arsenic species were used to explain adsorption behavior of As (III) and As (V) at different conditions. The Langmuir isotherm equations best interpreted the nature of adsorption of As (III) and A (V). It was found during phocatalytic process maximum R% was about 63% for As (III) using 40 mg photocatalyst.

* Corresponding author's E-mail address: kassaeem@modares.ac.ir

GRAPHICAL ABSTRACT

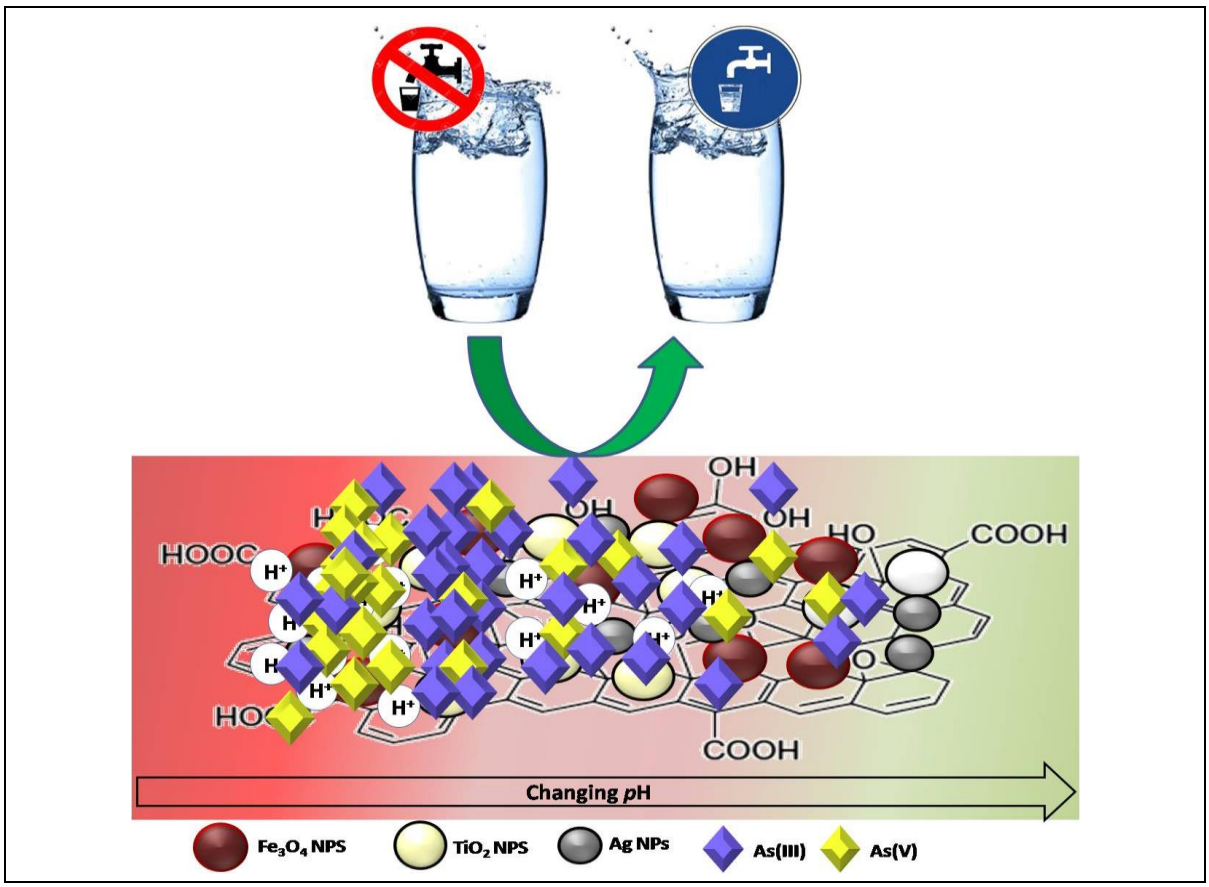

Introduction

Heavy metals have been known as water contaminants, even at permissible concentrations [1-4]. Among the heavy metals, arsenic is known as one of the most toxic metals in many parts of the world [5-7]. The main sources of arsenic are geological and human activities such as mining and pesticides. Arsenic may cause skin lesions and cancers of brain, liver, kidney, and stomach. Due to these detrimental effects very low level of arsenic in drinking water is highly desired [8, 9]. The maximum contaminant level (MCL) of arsenic in drinking water is about 50 µg/L in many countries [10]. The amount of As (III) and As (V) in water depends on the pH. The dominant form of arsenic in groundwater is the As (III), due to lower bonding to mineral surfaces [5-11].

There are many proposed technologies for As removal including sorption-ion exchange [12], oxidation precipitation [13], coagulation-coprecipitation [14], and membrane technologies such as ultrafiltration [15], nanofiltration [16], and reverse osmosis [9-17]. Among these methods adsorption techniques are commonly used. Nanoparticles (NPs) are promising materials with the advantage of high specific surface area, surface functional groups and suitable electric charge given by an adequate *Z*-potential [18]. On the other hand, hybrid materials have attracted a great deal of attention due to their availability in low cost and widespread application in water treatment [7]. Iron oxides or hydroxides [19], anatase TiO_2 and amorphous TiO_2 nanotube arrays [20,21], Fe_3O_4 and Fe_3O_4 NPs [22,23] have demonstrated excellent arsenic sorption characteristics. Combining nanomaterials with magnetic nanoparticles to separate adsorbents by an external magnetic field have

been considered [24]. Graphene oxide (GO) and functionalized graphene nanosheets have been suggested as a good support for other adsorbents [25-33].

Heterogeneous photocatalysis in aqueous media is an efficient way to oxidation of As (III) to As (V) [34-37].

Graphene [38], GO [39], graphene/TiO_2 [40,41], P25–graphene [42], P25/r-GO [43], GO/TiO_2 [41], graphene/various inorganic nanoparticles (Pt, Ni, Au, Ag, ZnO, CdS, and Fe_3O_4) [44-50], Ag/r-GO co-decorated TiO_2 nanotube arrays [51], and Ag/TiO_2/γ-Fe_2O_3@r-GO [52] have been reported as active photocatalysts.

Among the noble metals, Ag nanoparticles could improve the photocatalytic activity of TiO_2 as it may serve as a conductive bridge between r-GO and TiO_2 NPs [51]. Combination of Ag and r-GO serves as an electron acceptor and transporter [52].

The central composite design (CCD) which is the standard response surface methodology (RSM), allows estimating the second-degree polynomial of the relationships between the independent variables and the dependent variables [53-57]. In this work, arsenic removal by porous and magnetic Ag/TiO_2/Fe_3O_4@GO nanocomposite was assessed through adsorption and photocatalytic (without oxidant) process. The synergic effect of the presence of Ag nanoparticles on the adsorbent was investigated. The CCD was used for the experimental design to study the combined effects of different variables influencing the process. Monitoring of arsenic concentrations for evaluating R% and uptake capacity (q) of the adsorption process was done through application of inductively coupled plasma optical emission spectrometry (ICP-OES).

Experimental

Materials

Reagents for preparation of Ag/TiO_2/Fe_3O_4@GO nanocomposite are including natural flake graphite by Qingdao Dingding Graphite Products Factory, H_2SO_4 (98%), H_2O_2 (30%) and potassium permanganate ($KMnO_4$), $FeCl_3$. $6H_2O$ (98%), $FeCl_2$. $4H_2O$, (98%), $AgNO_3$ and $NaBH_4$ from Aldrich Co, and NH_4OH (25%) and tetrabutyl orthotitanate (TBOT) from Merck Co. $NaAsO_2$ was purchased from Merck Co. For As (V) solutions, $Na_2HAsO_4.7H_2O$ was obtained from Aldrich Co. All the purchased compounds were used as received, with no further purification.

The adsorbent was characterized by Fourier-transform infrared spectroscopy (FTIR) analysis using KBr pellets with a Thermo spectrometer, an X-ray diffraction analysis (XRD) (model Philips X'pert MPD, C_oK_α irradiation, λ = 1.78897 Å) at a scanning speed of 2°/min from 20° to 80° (2θ). Scanning electron microscope (SEM, model KYKY EM3200- 25 KV) and transmission electron microscope (TEM, model ZEISS, EM10C, 80 KV) were employed to evaluate the morphology of the synthesized materials. An ICP-OES (Inductively coupled plasma - optical emission spectrometry) was utilized to investigate the concentrations of As (III) and As (V) in solutions. Design-Expert 7.0.0 software was utilized for the experimental design.

GO was synthesized from natural graphite powder using a modified Hummers method [58]. In a typical procedure, 1 g of graphite was added to 100 mL of concentrated H_2SO_4 in an ice bath, and then 4 g of $KMnO_4$ was gradually added while stirring. The stirring was continued for 2 h at temperatures below 10 °C, followed by 1 h stirring at 35 °C until a thick paste was formed. Subsequently, it was diluted by 100 mL of deionized (DI) water in an ice bath and transferred to a 98 °C water bath and stirred for 1 h. The mixture was diluted again to 300 mL. Then, 20 mL of H_2O_2 (30%) was added to the mixture which changed the color to a brilliant yellow. The resultant was centrifuged and washed several times with 5% HCl, and then by

DI water until the pH of the supernatant becomes neutral. Finally the resulting solid was dried at 60 °C for 24 h, rendering a loose brown powder. 40 mg of the latter was ultrasonicated in of water (40 mL) for 30 min. A 50 mL solution of $FeCl_3$ (800 mg) and $FeCl_2$ (300 mg) (a molar ratio of 2:1) in DI water was added to it, at ambient. The temperature was gradually raised to 85 °C and a 30% ammonia solution was added till the *p*H increases to 10. After being rapidly stirred for 45 min the solution was cooled to room temperature. The resulting black precipitate was centrifuged at 4000 rpm for 15 min, washed three times with DI water and finally dried at 60 °C. The powder (Fe_3O_4@GO, 200 mg) was dispersed in of EtOH (20 mL) through ultrasonication for 30 min. TBOT (2 mL) was added to methyl acetoacetate (1 mL) and this mixture was added to Fe_3O_4@GO in EtOH at room temperature, in dark. $AgNO_3$ (200 mg) was dissolved in of EtOH (7 mL) and added to the resulting stable colloid. While stirring, distilled water (0.5 mL) was added drop wise. The mixture was stirred in dark for 4 h. The prepared gel was dried at 80 °C overnight. The resulting $Ag/TiO_2/Fe_3O_4$@GO was obtained after ball milling and calcinating of the dried nanocomposite at 350 °C for 2 h.

As (III)/As (V) removal procedure

The different variables on As (III) and As (V) removal from water were initial concentrations of arsenic ions, adsorbent/photocatalyst dosages, pH, and the time of contact. Using the method of CCD suggested 21 experimental runs (Tables 1 and 2). The experiments were carried out at room temperature by shaking a flask containing the desired dose of $Ag/TiO_2/Fe_3O_4$@GO nanocomposite in predetermined concentrations of As (III) (50 mL) for 30 min under no light source, and then at different time under the visible light.

For adsorption process, the batch adsorption experiments were carried out at room temperature by shaking a flask containing the desired dose of adsorbent in predetermined concentrations of As (III) or As (V) solution (50 mL).

Samples were withdrawn at different time intervals. The $Ag/TiO_2/Fe_3O_4$@GO nanocomposite was removed *via* a magnet and the remaining solution was analyzed for the residual As (III) or As (V) content *via* ICP-OES. Experiments were carried out at initial pH values ranging from 3 to 11. The initial pH was adjusted to the desired value either by HCl or NH_4OH solutions. The percent As (III) and As (V) removal (%R) was calculated using the Equation 1:

$$\%R = (1 - (C_i/C_0)) \times 100 \quad (1)$$

Where C_0 is the initial concentration of As (III) and As (V); and C_i is the final concentration of the latter. The adsorption capacity q_e (mg/g) after equilibrium was calculated using the mass balance relationship (Equation 2):

$$q_e = (C_0 - C_e)V/W \quad (2)$$

Where V is the volume of the solution (L) and W is the mass of adsorbent (g).

Table 1. Coded and actual values of the variables of the design of experiments for the As ions (III and V) removal optimization

Factor	Variables	Coded levels of variables				
		$-\alpha$	-1	0	+1	$+\alpha$
A	[As ions] (ppm)	6	12	18	24	30
B	Adsorbent (mg)	10	20	30	40	50
C	pH	3	5	7	9	11
D	Time (min)	45	90	135	180	225

Table 2. Experimental design and results of the central composite design

Std.	Conc. (ppm)	Adsorbent (mg)	pH	Time (min)	R% (Adsorption)	
					As (III)	As (V)
1	24	40	9	90	83.69	-
2	24	40	5	90	87.03	85.71
3	24	20	9	180	82.85	84.71
4	12	40	5	180	85.36	-
5	24	20	5	180	82.85	-
6	12	20	9	90	80.27	-
7	12	40	9	180	85.00	84.33
8	12	20	5	90	84.04	85.75
9	6	30	7	135	76.77	84.50
10	30	30	7	135	87.56	84.97
11	18	10	7	135	83.03	84.72
12	18	50	7	135	86.23	84.83
13	18	30	3	135	83.41	89.16
14	18	30	11	135	81.26	83.67
15	18	30	7	45	89.43	85.33
16	18	30	7	225	89.43	85.33
17	18	30	7	135	89.43	85.33
18	18	30	7	135	89.43	-
19	18	30	7	135	89.43	-
20	18	30	7	135	89.43	85.33
21	18	30	7	135	89.43	85.33

Results and discussion

Preparation and characterization of Nanocomposite

To prepare the $Ag/TiO_2/Fe_3O_4$@GO nanocomposite, Ag and TiO_2 nanoparticles were simultaneously dispersed on Fe_3O_4/GO nanocomposite using the sol-gel method. After calcination of the nanocomposite at 350 °C, TiO_2 crystallinity changed to the anatas form. The presence of the metallic Ag, anatase TiO_2, and Fe_3O_4 on the surface of GO were confirmed by XRD analysis and the EDX results revealed the existence of Ag, Ti, Fe, O and C elements (Figures 1 and 2). In the FT-IR spectrum of $Ag/TiO_2/Fe_3O_4$@GO, the absorption peaks around 474 cm^{-1} and 571 cm^{-1} were attributed to Ti–O and Fe–O bonds, respectively (Figure 3). Figure 4 demonstrates the TEM images of $Ag/TiO_2/Fe_3O_4$@GO nanocomposite consisted of darker color nano Ag, and the lighter Fe_3O_4 and TiO_2 nanoparticles. Higher magnifications showed 9 nm for average diameter of Ag nanoparticles. This suggested that TiO_2 and Ag nanoparticles were incorporated into the Fe_3O_4@GO system, forming our uniform $Ag/TiO_2/Fe_3O_4$@GO nanocomposite. Magnetic properties of $Ag/TiO_2/Fe_3O_4$@GO were investigated at room temperature (Figure 5).

Probing removal of As (III) and As (V) via CCD

The CCD with 21 runs (considering 5 center points) was employed to evaluate the combined effects of initial concentration of As (III) or As (V) (A), adsorbent dosage (B), pH (C), and contact time (D) on the percentage of arsenic removal in photo-catalytic and adsorption processes (Table 2).

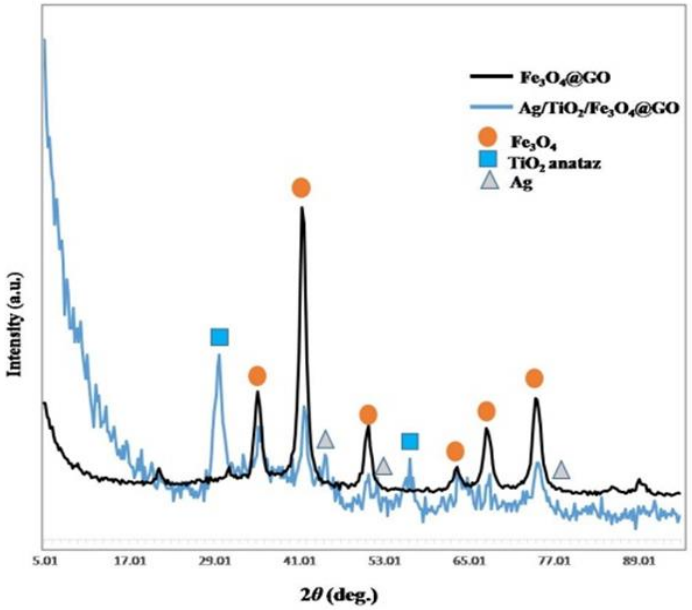

Figure 1. XRD patterns of our adsorbent: $Ag/TiO_2/Fe_3O_4@GO$

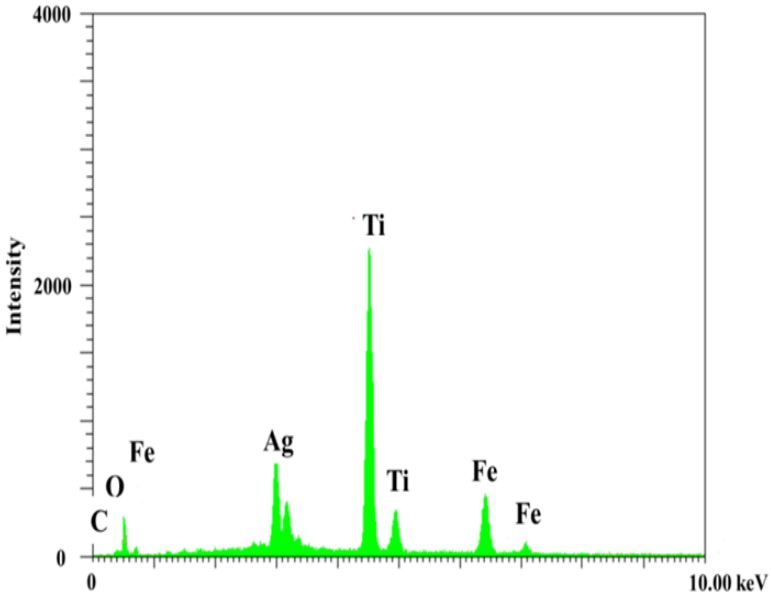

Figure 2. EDX spectrum of our adsorbent: $Ag/TiO_2/Fe_3O_4@GO$

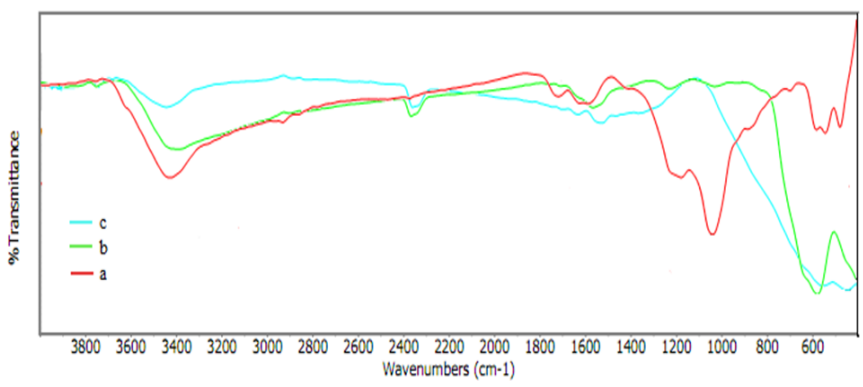

Figure 3. IR Spectra of synthesized GO (a), Fe_3O_4@ GO (b), and $Ag/TiO_2/Fe_3O_4@GO$ nanocomposite (c)

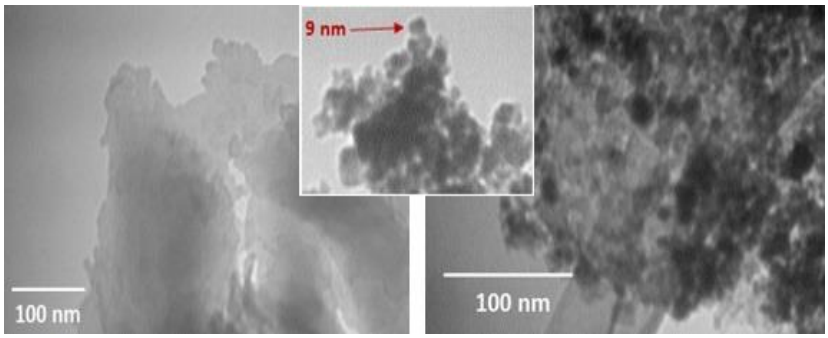

Figure 4. TEM images of synthesized GO (a), $Ag/TiO_2/Fe_3O_4$@GO nanocomposite (b)

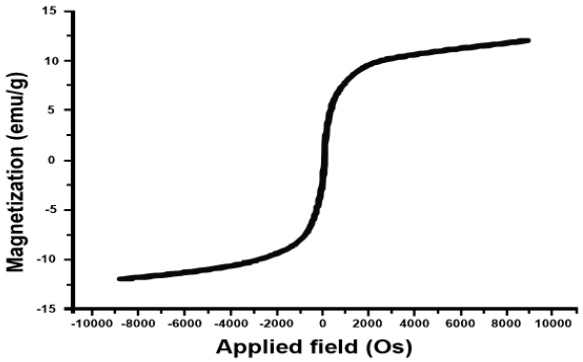

Figure 5. Magnetization curve of magnetic $Ag/TiO_2/Fe_3O_4$@GO nanocomposite

The phocatalytic process maximum R% for As (III) was about 63% with 40 mg photocatalyst during 90 min in pH 5, while any photocatalytic activity was not observed with less than 40 mg catalyst. That might be due to covering all the active sites on catalyst by arsenic species especially $H_2AsO_3^-$ which happen through the adsorption process.

For adsorption process, polynomial equations were validated by conducting the variance (ANOVA) to determine the significance of each term in equation and estimate the goodness of fit in each case. Based on the ANOVA results for quadratic model, CCD suggested second order polynomial equation for treatment of As (III) as following equation:

$$R\% = 89.43 + 2.70A + 0.8B - 0.74C + 0.0D - 0.13AB + 0.10\ AC - 0.58AD + 8.406*10^{-3}BC + 2.48BD + 0.84CD - 1.\ 91A^2 - 1.29B^2 - 1.87C^2 - 0.094D^2 \quad (3)$$

Effects of A-D parameters on As (III) removal efficiency (y^2) were summarized on 3D surface plots (Figure 6).

Effects of initial concentration of As (III) was greater than that of the others variables (A>B>C>D). Coefficient of regression (R^2) was used as an important parameter to check the adequacy of the model. According to Joglekar and May [60] R^2 should be at least 0.80 for good fitting of a model. The value of R^2 for removal of As (III) was 0.99, showed an excellent agreement between the actual and predicted values of the As (III) adsorption on $Ag/TiO_2/Fe_3O_4$@GO nanocomposite (Figure 7).

A regression analysis of the model equation demonstrated that the main effects as well as their interaction were highly significant (P-value<0.0001) (Table 3). Applying the quadratic model showed the optimum values of A, B, C, and D as 24 ppm, 20 mg, 5, and 90 min, respectively. This led to a removal efficiency (R%) of 91. Overlay plot suggested that A and B should appear in the yellow area in order to obtain 88<R%<100 (Figure 8).

For As (V) removal, the adsorption was complete within the first few minutes of the experiments so that the time factor was assumed to be constant (30 min). Therefore,

the designs were optimized and only the fifteen runs specified in Table 2 were considered for optimal conditions. The ANOVA validated model provided P-value<0.0001 and R^2 = 0.93 (Table 4). The actual values *vs.* predicted values of the As (V) adsorption through Ag/TiO_2/Fe_3O_4@GO nanocomposite indicated an excellent agreement between them (Figure 9).

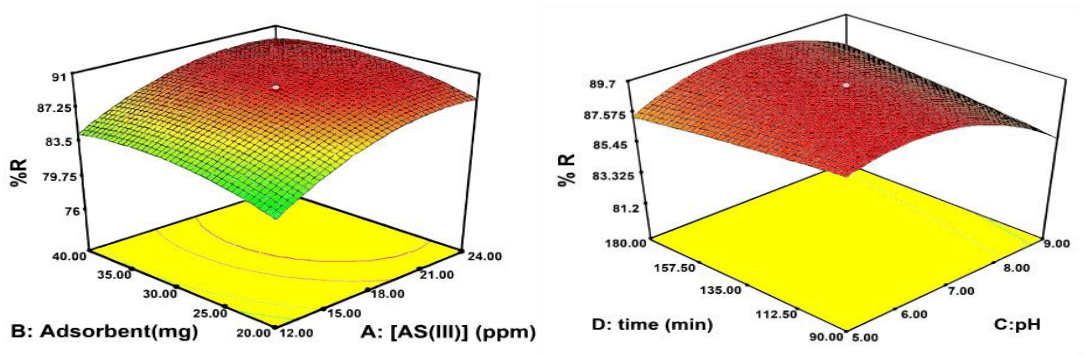

Figure 6. 3D surface plots showing the effects of the initial concentration of As (III) (A), amount of adsorbent (B), the initial *p*H (C), and time (D) on As (III) removal efficiency (y^2)

Figure 7. Actual values *vs.* predicted values of the As (III)

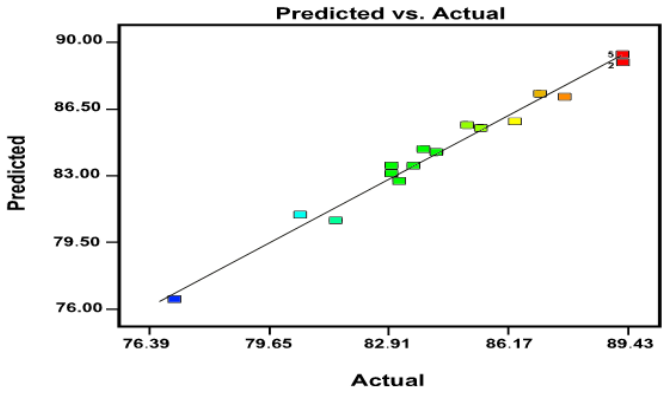

Table 3. ANOVA for response surface quadratic model for As (III) removal

Source	Sum of squares	df	Mean square	F Value	p-value Prob>F	
Model	264.0649	14	18.86178	39.01612	0.0001	Significant
A-[As ions]	58.21205	1	58.21205	120.4133	< 0.0001	
B-Adsorbent	5.12	1	5.12	10.59087	0.0174	
C-pH	8.658306	1	8.658306	17.90995	0.0055	
D-time	0	1	0	0	1.0000	
AB	0.066306	1	0.066306	0.137156	0.7238	
AC	0.078013	1	0.078013	0.161371	0.7018	
AD	1.363056	1	1.363056	2.819521	0.1441	
BC	0.000613	1	0.000613	0.001267	0.9728	
BD	24.57681	1	24.57681	50.83783	0.0004	
CD	5.695313	1	5.695313	11.78092	0.0139	
A^2	91.6051	1	91.6051	189.4878	< 0.0001	
B^2	42.03927	1	42.03927	86.95943	< 0.0001	
C^2	87.57477	1	87.57477	181.1509	< 0.0001	
D^2	0.2228	1	0.2228	0.460867	0.5225	
Residual	2.900613	6	0.483435			
Lack of Fit	2.900613	2	1.450306			
Pure Error	0	4	0			

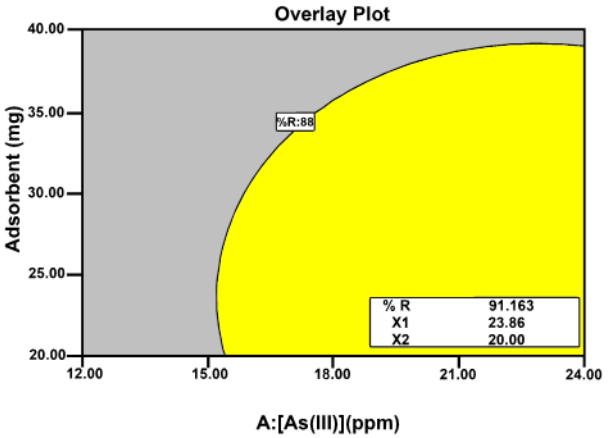

Figure 8. Overlay plot for As (III) adsorption by $Ag/TiO_2/Fe_3O_4$@GO nanocomposite

$$R\% = 85.09 + 9.37\times10\text{-}3A' + 0.14B' - 1.16C' - 0.35A'B' + 0.36A'C' - 0.18B'C' - 0.13A'^2 - 0.12B'^2 + 0.29C'^2 \quad (4)$$

The graphical 3D surface plots represented simultaneous effects of the initial concentration of As (V) (A′), amount of adsorbent (B′), and the initial pH (C′) on As (V) removal efficiency (y^2) as the response factor (Figure 10).

Model response equations based on ANOVA results revealed that, the effects of pH was more than others (C′>B′>A′). Based on quadratic model to reach R% = 87% efficiency, the optimum values of A′, B′, and C′ were 17 ppm, 11 mg, and 3, respectively. The optimum contact time for As (V) removal was not obtained from the quadratic model because it was omitted from the model. To obtain 87<R%<100 A′ and B′ should appear in the yellow area in the overlay plot (Figure 11).

The removal capacity of $Ag/TiO_2/Fe_3O_4$@GO nanocomposite for As (III) was enhanced as the *p*H increased from 3 to 8. The removal efficiency of As (III) reached 91% at *p*H 5 for our adsorbent (Figure 6). At pH less than 3, H_3AsO_3 are major non-anionic species of As (III) and its adsorption on the surface of nanocomposite is less than anionic species. At pH more than 8, the positive charge on adsorbent surfaces decrease and the removal efficiency of As (III) could be reduced. The adsorption of As (V) was affected by changing pH, so that raising the initial pH reduced the removal efficiency of the As (V) (as seen in Figure 10). Under most of the pH conditions, As (V) existed in negative ionic form, $H_2AsO_4^-$ [61]. On the other hand, at low pH, H^+ could easily interact with the negative charges on Ag NPs surface, oxygen groups in TiO_2 and Fe_3O_4 NPs, and functional groups on GO to form surface complexes [62,63]. So, the electrostatic attraction of the negatively charged $H_2AsO_4^-$ species on the positively charge sites of adsorbent caused higher adsorption of As (V) at lower pH.

Removal of As (III) and As (V) enhanced by increasing the amount of adsorbent due to the increase in contact surface of the adsorbent (Figures 6 and 10). The latters might bind to hydroxide (–OH), epoxide (–O–) and carboxylic (–COOH) groups on the GO nanosheets [64] and to FeOOH which produced from Fe_3O_4 in aqueous medium as a highly reactive iron species [54]. Moreover, a large number of silver atoms existed on or near the adsorbent surface and in optimum pH, the surface charge of AgNPs is positive. In addition, an increase in the distribution of active sites on Ag nanostructured surface might happen because of lack of internal diffusion resistance that lead to high adsorptive capacity [55]. Furthermore, arsenic ions species could be adsorbed on TiO_2 because adsorption onto TiO_2 played an important role during the photocatalytic reactions [65].

As seen in Figures 6 and 10 increasing the initial concentrations of As (III) and As (V) improved the adsorption. It might be due to the

fact that As ion species at optimum *p*H could easily interact with adsorbent surface, producing coagulated species. It increased aggregation of nanocomposite with adsorbent and finally R% of As (III) and As (V) (Figure 12).

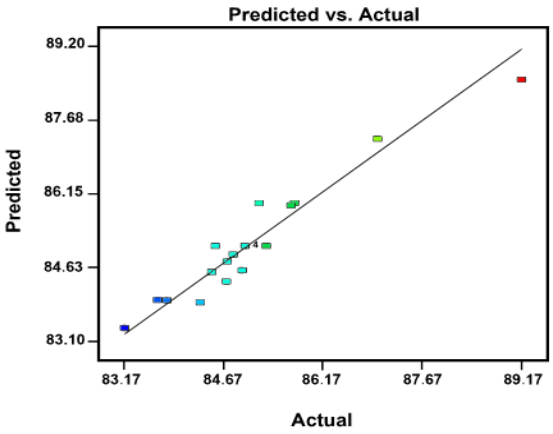

Figure 9. Actual values *vs*. predicted values of the As(V)

Table 4. ANOVA for response surface quadratic model for As (V) removal

Source	Sum of squares	df	Mean square	F Value	p-value Prob>F	
Model	20.41013	9	2.267792	113.3846	< 0.0001	Significant
A-[As ions]	0.11045	1	0.11045	5.522258	0.0656	
B-Adsorbent	0.00605	1	0.00605	0.302487	0.6060	
C-pH	15.07005	1	15.07005	753.4695	< 0.0001	
AB	1.570817	1	1.570817	78.53739	0.0003	
AC	0.046817	1	0.046817	2.340731	0.1866	
BC	0.002817	1	0.002817	0.140827	0.7229	
A^2	0.58884	1	0.58884	29.44073	0.0029	
B^2	0.516964	1	0.516964	25.84704	0.0038	
C^2	1.59684	1	1.59684	79.83852	0.0003	
Residual	0.100004	5	0.020001			
Lack of Fit	0.100004	1	0.100004			
Pure Error	0	4	0			
Cor Total	20.51013	14				

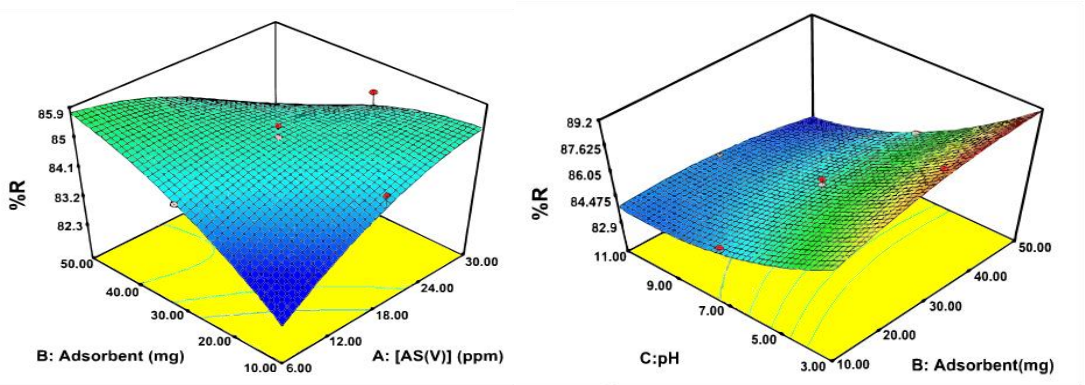

Figure 10. 3D surface plots showing the effects of the initial concentration of As(V) (A), amount of adsorbent (B), on As(V) removal efficiency (y^2)

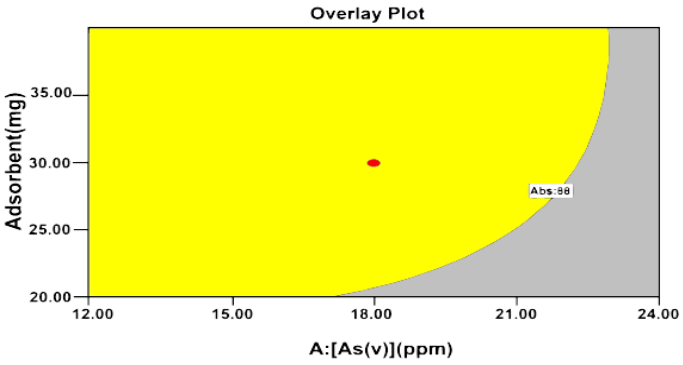

Figure 11. Overlay plot for As(V) adsorption by our adsorbent: $Ag/TiO_2/Fe_3O_4$@GO nanocomposite

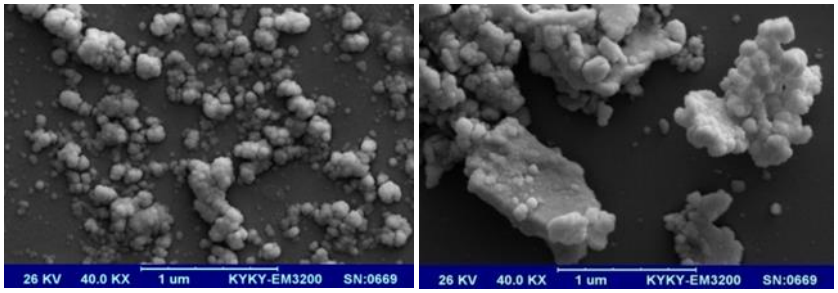

Figure 12. SEM images of $Ag/TiO_2/Fe_3O_4$@GO before using (left) and after using as adsorbent (right)

Adsorption isotherms

The equilibrium relationships between our adsorbent and As (III/V) explained using the Freundlich and Langmuir isotherm models [66]. The studies were recorded by varying the initial concentration of As (III) and As (V) solution from 6 mg/L to 30 mg/L. The Freundlich model is stated as:

$$\log q_e = \log K_F + (1/n)\log C_e \quad (5)$$

Here C_e denotes the equilibrium concentration (mg/L^{-1}) of As (III/V), q_e is the amount adsorbed (mg/g^{-1}), and K_F and n are the Freundlich constants related to the adsorption capacity and adsorption intensity, respectively. The Freundlich constants for our adsorbent and As (III) and As (V) were calculated (Figure 13a and Table 5).

The Langmuir isotherm for our system is stated as:

$$1/q_e = 1/Q_o + 1/(bQ_oC_e) \quad (6)$$

Where C_e denotes the equilibrium concentration of the adsorbent (mg/L^{-1}), q_e is the amount adsorbed (mg/g^{-1}), Q_0 is the adsorption capacity (mg/g^{-1}), and b signifies the energy of adsorption (L/mg^{-1}). Langmuir constants were calculated using plot of $1/q_e$ against $1/C_e$, in pH = 7, at room temperature for As (III) and As (V) (Figure 13b and Table 5).

Separation factor 'r', the dimensionless parameter of equilibrium [66], was calculated using the Equation 7.

$$r = 1/(1 + bC_0) \quad (7)$$

Where C_0 is the initial concentration and b signifies the Langmuir constant. The separation factor in each initial concentration (C_0) was calculated (Table 6).

On comparing the regression coefficients obtained for Freundlich and Langmuir isotherms, it could be predicted that in pH = 7, Langmuir isotherm was more favored for As (III) and As (V), indicating that a mono-layer of As (III) and As (V) was formed.

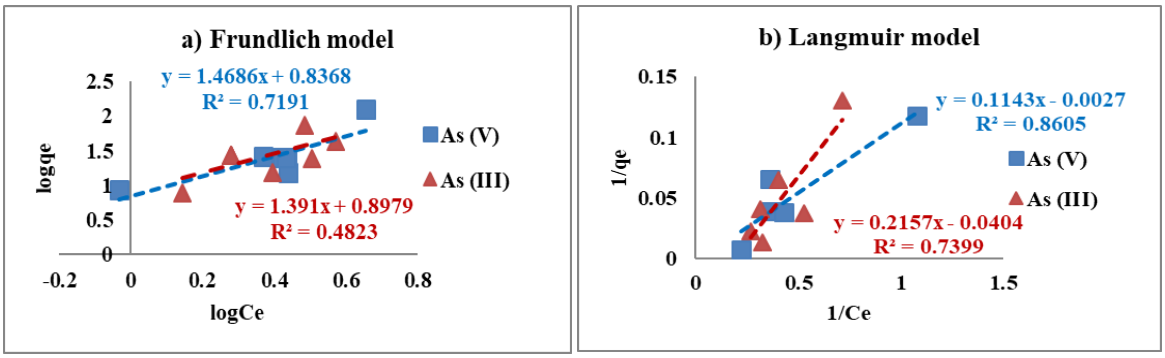

Figure 13. Freundlich (a) and Langmuir, (b) adsorption isotherms for the As (III)/As (V)–Ag/TiO_2/Fe_3O_4@GO system at pH = 7

Table 5. The Frundlich and Langmuir constants for As (III) and As (V)

	Frundlich constants		Langmuir constants	
	K_F	n	Q_o	b
As (III)	7.9	0.72	-24.75	-0.187
As (V)	6.87	0.68	-370.37	-0.024

Table 6. Separation factor for As (III) and As (V) in each initial concentrations

C_0	r (As (III))	r (As (V))
6	-8.08	1.16
12	-0.80	1.39
18	-0.42	1.74
24	-0.29	2.31
30	-0.22	3.43

Conclusion

In this work, we presented a simple method to prepare porous magnetic Ag/TiO_2/Fe_3O_4@GO nanocomposite. The results demonstrated a high adsorption capacity for the As (III) using 20 mg adsorbent, 24 ppm initial concentration of As (III), at pH = 5, within 90 min, and room temperature. It showed good adsorption for As(V) applying 11 mg adsorbent, 17 ppm initial concentration of As (V), at pH = 3, within 30 min, and room temperature. Maximum R% for As (III) was about 63% during phocatalytic process. A CCD, for four factors and five center points for As (III) and three factors and five center points for As (V) explained the system's behavior by the empirical second-order polynomial equation in each case. The equilibrium relationships between nanocomposite and adsorbent were explained by Langmuir, and Freundlich adsorption isothermal models. Langmuir isotherm was more favorable for As (III) and As (V) removal.

Acknowledgement

The authors are grateful to the Iran National Science Foundation (INSF) for supporting this work.

Compliance with ethical standards

On behalf of all authors, the corresponding author states that there is no conflict of interest.

This article does not contain any studies with human participants or animals performed by any of the authors.

This study was funded by Iran National Science Foundation (INSF).

ORCID

M. Z. Kassaee **:** 0000-0001-6840-6806

References

[1] H. Noorizadeh, A. Farmany, *Adv. J. Chem. A*, **2019**, *2*, 128–135.

[2] M. Kumari, C.U. Pittman, D. Mohan, *J. Coll. Interface Sci.,* **2015**, *442*, 120-132.

[3] C.G. Fraga, *Mol. Aspects .Med.,* **2005**, *26*, 235–244.

[4] L. Järup, *Br. Med. Bull.*, **2003**, *68*, 167-182.

[5] J.I. Garza-Arévalo, I. García-Montes, M.H. Reyes, J.L. Guzmán-Mar, V. Rodríguez-González, L.H. Reyes, *Mat. Res. Bullet.*, **2016**, *73*,145–152.

[6] X. Xie, K. Pi, Y. Liu, C. Liu, J. Li, Y. Zhu, C. Su, T. Ma, Y. Wang, *China, J. Hazard. Mater.,* **2016**, *302*, 19–26.

[7] S. Mandal, S.S. Mahapatra, M.K. Sahu, R.K. Patel, *Process. Saf. Environ.,* **2015**, *93*, 249–264.

[8] K.S. Abdul, S.S. Jayasinghe, E.P. Chandana, C. Jayasumana, P.M. De-Silva, *Environ. Toxicol. Pharmacol.,* **2015**, *40*, 828–846.

[10] S.I. Siddiqui, S.A. Chaudhry, *Curr. Environ. Eng.,* **2017,** *4*, 81–102.

[11] B. An, H. Kim, C. Park, S.H. Lee, J.W. Choi, *J. Hazard. Mater.*, **2015**, *289*, 54–62.

[12] S. Zavareh, M. Zarei, F. Darvishi, H. Azizi, *Chem. Eng. J.*, **2015**, *273*, 610–621.

[13] M.R. Awual, M.A. Shenashen, T. Yaita, H. Shiwaku, A. Jyo, *Water Res.*, **2012**, *46*, 5541–5550.

[14] H. Yanga, W. Sun, H. Ge, R. Yao, *Environ. Tech.*, **2015**, *36*, 2732–2739.

[15] C.Y. Hu, S.L. Lo, W.H. Kuan, *Sep. Purific. Tech.,* **2014**, *126*, 7–14.

[16] H.R. Lohokare, M.R. Muthu, G.P. Agarwal, U.K. Kharul, *J. Membrane. Sci.*, **2008**, *320*, 159–166

[17] P. Pal, S. Chakrabortty, L. Linnanen, *Sci. Total Environ.,* **2014**, *476-477*, 601–610.

[18] F. Chang, W. Liu, X. Wang, *Desalination*, **2014**, *334*, 10–16.

[19] A.R. Contreras, A. Garcı´a, E. Gonza´lez, E. Casals, V. Puntes, A. Sa´nchez, X. Font, S. Recillas, *Desalin. Water Treat.,* **2012**, *41*, 296–300.

[20] W. Chen, R. Parette, J. Zou, F.S. Cannon, B.A. Dempsey, *Water Res.*, **2007**, *41*, 1851–1858.

[21] S. Wu, W. Hu, X. Luo, F. Deng, K. Yu, S. Luo, L. Yang, X. Tu, G. Zeng, *Environ. Tech.*, **2013**, *34*, 2285–2290.

[22] G.M. Kuz'micheva, E.V. Savinkina, L.N. Obolenskaya, L.I. Belogorokhova, B.N. Mavrin, M.G Chernobrovkin, A.I. Belogorokhov, *Crystall. Rep.,* **2010**, *55*, 866–871.

[23] I. Akin, G. Arslan, A. Tor, M. Ersöz, Y. Cengeloglu, *J. Hazard. Mat.*, **2012**, *62*, 235–236.

[24] H. Thacker, V. Ram, P.N. Dave, *Prog. Chem. Biochem. Res.,* **2019**, *2*, 84–91.

[25] J. Lan, *Res. Chem. Intermed.,* **2015**, *41*, 3531–3541.

[26] L. Guoa, P. Ye, J. Wang, F. Fua, Z. Wu, *J. Hazard. Mater.,* **2015**, *298*, 28–35.

[27] A.K. Mishra, S. Ramaprabhu, *Desalination*, **2011**, *282*, 39–45.

[28] L. Li, G. Zhou, Z. Weng, X.Y. Shan, F. Li, M.H. Cheng, *Carbon*, **2014**, *67*, 500–507.

[29] K. Zhang, V. Dwivedi, C. Chi, J. Wu, *J. Hazard. Mater.,* **2010**, *182*, 162–168.

[30] G. Sheng, Y. Li, X. Yang, X. Ren, S. Yang, J. Hu, X. Wang, *RSC Adv.,* **2012**, *2*, 12400–12407.

[31] V. Chandra, J. Park, Y. Chun, J.W. Lee, I.C. Hwang, K.S. Kim, *ACS Nano*., **2010**, *4*, 3979–3986.

[32] T. Wen, X. Wu, X. Tan, X. Wang, A. Xu, *ACS Appl. Mater. Interfaces,* **2013**, *5*, 3304–3311.

[33] X.L. Wu, L. Wang, C.L. Chen, A.W. Xu, X.K. Wang, *J. Mater. Chem*., **2011**, *21*, 17353–17359.

[34] X. Luo, C. Wang, S. Luo, R. Dong, X. Tu, G. Zeng, *Chem. Eng. J.*, **2012**, *187*, 45–52.

[35] M. Bissen, M.M. Vieillard-Baron, A.J. Schindelin, F.H. Frimmel, *Chemosphere*, **2001**, *44*, 751–757.

[36] H. Lee, W. Choi, *Environ. Sci. Technol.,* **2002**, *36*, 3872–3878.
[37] P.M. Jayaweera, P.I. Godakumbra, K.A.S. Pathiartne, *Curr. Sci. India*, **2003**, *84*, 541–543.
[38] A.H. Fostier, M.S.S. Pereira, S. Rath, J. R. Guimara˜es, *Chemosphere,* **2008**, *72*, 319–324.
[39] S. Morales-Torres, L.M. Pastrana-Martínez, J.L. Figueiredo, J.L. Faria, A.M.T. Silva, *Appl. Surface Sci.,* **2013**, *275*, 361–368.
[40] G. Vinodhkumar, R. Ramya, M. Vimalan, I. Potheher, A. Cyrac Peter, *Prog. Chem. Biochem. Res.,* **2018**, *1*, 40–49.
[41] Q. Huang, S. Tian, D. Zeng, X. Wang, W. Song, Y. Li, W. Xiao, C. Xie, *ACS Catal*., **2013**, *3*, 1477–1485.
[42] P. Wang, Y. Zhai, D. Wang, S. Dong, *Nanoscale,* **2011**, *3*, 1640–1645.
[43] H. Zhang, X. Lv, Y. Li, Y. Wang, J. Li, *ACS Nano.,* **2010**, *4*, 380–386.
[44] W.Q. Fan, Q.H. Lai, Q.H. Zhang, Y. Wang, *J. Phys. Chem. C*, **2011**, *115*, 10694–10701.
[45] Y. Qian, C.Y. Wang, Z.G. Le, *Appl. Surface Sci.,* **2011**, *257*, 10758–10762.
[46] C. Xu, X. Wang, J.W. Zhu, *J. Phys. Chem. C*, **2008**, *112*, 19841–19845.
[47] J. Yang, C.L. Zang, L. Sun, N. Zhao, X.N. Cheng, *Mater. Chem. Phys.*, **2011**, *129*, 270–274.
[48] Z.Y. Gao, N. Liu, D.P. Wu, W.G. Tao, F. Xu, K. Jiang, *Appl. Surface Sci.,* **2012**, *258*, 2473–2478.
[49] J.C. Liu, L. Liu, H.W. Bai, Y.J. Wang, D.D. Sun, *Appl. Catal. B Environ*., **2011**, *106*, 76–82.
[50] G.M. Zhou, D.W. Wang, F. Li, L.L. Zhang, N. Li, Z.S. Wu, L. Wen, G.Q. Lu, H.M. Cheng, *Chem. Mater.,* **2010**, *22*, 5306–5313.
[51] Y. Yang, T.X. Liu, *Appl. Surface Sci.,* **2011**, *257*, 8950–8954.
[52] Y. Tang, S. Luo, Y. Teng, C. Liu, X. Xu, X. Zhang, L. Chen, *J. Hazard. Mater.,* **2012**, *241–242*, 323–330.
[53] M. Ghavami, R. Mohammadi, M. Koohi, M.Z. Kassaee, *Mat. Sci. Semicon. Proc.,* **2014**, *26*, 69–78.
[54] M. Khazaei, S. Nasseri, M.R. Ganjali, M. Khoobi, R. Nabizadeh, A.H. Mahvi, S. Nazmara, E. Gholibegloo, *J. Environ. Health Sci. Eng.*, **2016**, *14*, 2.
[55] R. Yongsheng, L. Jun, D. Xiaoxiao, *Canadian J. Chem. Eng.*, **2011**, *89*, 491–498.
[56] J.P. Wang, Y.Z. Chen, X.W. Ge, H.Q. Yu, *Colloids Surf. A Physicochem. Eng*., **2007**, *302*, 204–210.
[57] S.S. Hosseiny Davarani, Z. Rezayati zad, A. Taheri, N. Rahmatian, *Mater. Sci. Eng. C.,* **2017**, *71*, 572–583.
[58] K. Kamari, A. Taheri, *J. Taiwan Inst. Chem. Eng.,* **2018**, *86*, 230–239.
[59] W.S. Hummers, R.E. Offeman, *J. Am. Chem. Soc.*, **1958**, *80*, 1339–1339.
[60] P. Roy, U. Dey, S. Chattoraj, D. Mukhopadhyay, N.K. Mondal, *Appl. Water Sci.*, **2017**, *7*, 1307–1321.
[61] S.L. Ferreira, R.E. Bruns, H.S. Ferreira, G.D. Matos, J.M. David, G.C. Brenda, E.G.P. da Silva, L.A. Portugal, P.S. dos Reis, A.S. Souza, W.N.L. dos Santos, *Anal. Chim. Acta.,* **2007**, *597*, 179–186.
[62] F. Perreault, A.F. De Faria, M. Elimelech, *Chem. Soc. Rev*., **2015**, *44*, 5861–5896.
[63] C. Cheng, Z. Liu, X. Li, B. Su, T. Zhou, C. Zhao, *RSC Adv.*, **2014**, *4*, 42346–42357.
[64] S.A. Baig, T.T. Sheng, C. Sun, L.S. Xue, Z.Q. Tan, X.H. Xu, *PLOS ONE*, **2014**, *9,* e100704.
[65] K. Dastafkan, M. Khajeh, M. Bohlooli, M. Ghaffari-Moghaddam, N. Sheibani, *Talanta*, **2015**, *144*, 1377–1386.
[66] A. Mittal, J. Mittal, A. Malviya, D. Kaur, V.K. Gupta, *J. Coll. Interface Sci*., **2010**, *343*, 463–473.

How to cite this manuscript: M. Miranzadeh, F. Afshari, B. Khataei, M.Z. Kassaee, Adsorption and Photocatalytic Removal of Arsenic from Water by a Porous and Magnetic Nanocomposite: Ag/TiO2/Fe3O4@GO, *Adv. J. Chem. A*, **2020**, *3*(4), 408–421.